Determining the Nuclear Gluon Distribution in UPCs

R. Vogt

Nuclear Science Division, LBNL, Berkeley, CA, USA
Physics Department, University of California, Davis, CA, USA

- Heavy Quark Photoproduction–Direct and Resolved
- Dijet Photoproduction–Direct

Photoproduction Comes For Free in Heavy Ion Collisions

- **Strong electromagnetic fields surround accelerated nuclei**
- **Photon from field of one nucleus interacts with gluon from periphery of opposite nucleus**
- **Photons almost real, virtuality $q^2 < (\hbar c/R_A)^2$, small**
- **These photons can interact themselves (direct) or fluctuate into states with multiple $q\overline{q}$ pairs and gluons (resolved)**
- **Grazing collisions with rapidity gap could be clean signal for photoproduction measurements**

Kinematics

Photon beam is not monotonic but a continuum up to

$$E_{\rm beam} = \gamma_L m_p$$

Relate photon 4-momentum to x_1 as in hadroproduction,

$$k = x_1 \gamma_L m_p$$

x_1 **and** x_2 **depend on the** p_T **and** y **of the produced quarks**

$$x_2 = (m_T/\sqrt{S})(e^{y_1} + e^{y_2}) \qquad x_1 = (m_T/\sqrt{S})(e^{-y_1} + e^{-y_2})$$

Photon flux suppressed for $k_{\rm max} = \gamma_L \hbar c/R_A$ in the center of mass frame, and $E_{\rm cut} = (2\gamma_L^2 - 1)\hbar c/R_A$ in lab frame

Maximum possible $\gamma - N$ center-of-mass energy, $\sqrt{S_{\gamma N}}$, less than $\sqrt{S}$ in corresponding NN collisions

$$\sqrt{S_{\gamma N}} = 2\sqrt{k_{\rm max} E_{\rm beam}} = m_p^2 + 2 m_p E_{\rm cut}$$

Some Numbers

A	E_{beam} (GeV)	γ_L	k_{max} (GeV)	E_{cut} (TeV)	$\sqrt{S_{\gamma N}}$ (GeV)
			RHIC		
O	125	133	8.7	2.31	66
Si	125	133	7.2	1.92	60
I	104	111	3.6	0.81	39
Au	100	106	3.0	0.66	35
			AA LHC		
O	3500	3730	357.3	1820	1850
Ar	3150	3360	185.7	1080	1430
Pb	2750	2930	87	480	950
			pA LHC		
O	4950	5270	435.4	3630	2610
Ar	4700	5000	276.4	2410	2130
Pb	4400	4690	139.2	1220	1500

Table 1: Beam energies, E_{beam}, Lorentz factors, γ_L, photon cutoff energy in the lab frame, k_{max}, and in the nuclear rest frame, E_{cut}, as well as the equivalent NN center-of-mass energy for E_{cut}, $\sqrt{S_{\gamma N}}$, for AA collisions at RHIC and AA and pA collisions at the LHC.

Photon Flux

Weizsäcker-Williams flux function of distance from the nucleus, r,

$$\frac{d^3N_\gamma}{dkd^2r} = \frac{Z^2\alpha w^2}{\pi^2 k r^2}\left[K_1^2(w) + \frac{1}{\gamma_L^2}K_0^2(w)\right]$$

$w = kr/\gamma_L$, $K_0(w)$ **and** $K_1(w)$ **are modified Bessel functions**

Total flux is integral over transverse area of the target assuming nuclei do not interact, $r > 2R_A$ **for** AA **and** $r > r_p + R_A$ **for** pA**,**

$$\frac{dN_\gamma}{dk} = \frac{2Z^2\alpha}{\pi k}\left[w_R^{iA}K_0(w_R^{iA})K_1(w_R^{iA}) - \frac{(w_R^{iA})^2}{2}(K_1^2(w_R^{iA}) - K_0^2(w_R^{iA}))\right]$$

$w_R^{AA} = 2kR_A/\gamma_L$, $w_R^{pA} = 2k(r_p + R_A)/\gamma_L$

We numerically evaluate the flux taking into account the nuclear shapes for AA **collisions but use the analytical result for** pA

AA **evaluations agree best when** $kR_A/\gamma_L\hbar c \ll 1$ **or** $M/\sqrt{S_{\gamma N}}$ **is small**

At LHC, analytical and numerical results agree within 8%

Direct $Q\overline{Q}$ Photoproduction

Hadronic reaction: $\gamma(k)+N(P_2) \to Q(p_1)+\overline{Q}(p_2)+X$

LO partonic reaction: $\gamma(k) + g(x_2P_2) \to Q(p_1) + \overline{Q}(p_2)$

Partonic cross section

$$s^2\frac{d^2\sigma_{\gamma g}}{dt_1du_1} = \pi\alpha_s(Q^2)\alpha e_Q^2\left(\frac{t_1}{u_1}+\frac{u_1}{t_1}+\frac{4m^2s}{t_1u_1}\left[1-\frac{m^2s}{t_1u_1}\right]\right)\delta(s+t_1+u_1)$$

Partonic invariants: $s = (k+x_2P_2)^2 = 4kx_2m_p\gamma_L$, $t_1 = (x_2P_2-p_1)^2 - m^2$, $u_1 = (k-p_1)^2 - m^2$

Couplings: $\alpha = e^2/\hbar c$, $\alpha_s(Q^2) \approx 0.11$, $e_c = e_t = 2/3$, $e_b = -1/3$

Hadronic cross section, convolution over gluon density, photon flux

$$S^2\frac{d^2\sigma_{\gamma A\to Q\overline{Q}X}}{dT_1dU_1d^2b} = 2\int dz\int_{k_{\rm min}}^{\infty} dk\frac{d^3N_\gamma}{dkd^2b}\int_0^1\frac{dx_2}{x_2}F_g^A(x_2,Q^2,\vec{b},z)s^2\frac{d^2\sigma_{\gamma g}}{dt_1du_1}$$

Minimum photon momentum for pair of mass M **is** $k_{\rm min} = M^2/(4\gamma_L m_p)$

Hadronic invariants: $S = (k+P_2)^2$, $T_1 = (P_2-p_1)^2-m^2$, $U_1 = (k-p_1)^2-m^2$

Factor of two because both nuclei can be targets

Resolved Photoproduction

LO partonic reaction:

$$g(xk) + g(x_2 P_2) \rightarrow Q(p_1) + \overline{Q}(p_2)$$
$$q(xk) + \overline{q}(x_2 P_2) \rightarrow Q(p_1) + \overline{Q}(p_2)$$

Partonic cross sections

$$\hat{s}^2 \frac{d^2\sigma_{q\overline{q}}}{d\hat{t}_1 d\hat{u}_1} = \pi\alpha_s^2(Q^2)\frac{4}{9}\left(\frac{\hat{t}_1^2 + \hat{u}_1^2}{\hat{s}^2} + \frac{2m_Q^2}{\hat{s}}\right)\delta(\hat{s} + \hat{t}_1 + \hat{u}_1)$$

$$\hat{s}^2 \frac{d^2\sigma_{gg}}{d\hat{t}_1 d\hat{u}_1} = \frac{\pi\alpha_s^2(Q^2)}{16}\left(\frac{t_1}{u_1} + \frac{u_1}{t_1} + \frac{4m_Q^2 s}{t_1 u_1}\left[1 - \frac{m_Q^2 s}{t_1 u_1}\right]\right)\left[3\left(1 - \frac{2\hat{t}_1\hat{u}_1}{\hat{s}^2}\right) - \frac{1}{3}\right]\delta(\hat{s} + \hat{t}_1 + \hat{u}_1)$$

Partonic invariants: $\hat{s} = (xk + x_2 P_2)^2$, $\hat{t}_1 = (x_2 P_2 - p_1)^2 - m^2$, $\hat{u}_1 = (xk - p_1)^2 - m^2$

Resolved cross sections are factor $\alpha_s(Q^2)/(\alpha e_Q^2)$ larger

Now convolute over parton distributions in the photon too

$$S^2 \frac{d^2\sigma^{\rm res}_{\gamma A \rightarrow Q\overline{Q}X}}{dT_1 dU_1 d^2b} = 2\int dz \int_{k_{\rm min}}^{\infty} dk \frac{d^3 N_\gamma}{dk db^2} \int_{\frac{k_{\rm min}}{k}} \frac{dx}{x} \int_{x_{2_{\rm min}}}^{1} \frac{dx_2}{x_2} \left[F_g^\gamma(x, Q^2) F_g^A(x_2, Q^2, \vec{b}, z) \hat{s}^2 \frac{d^2\sigma_{gg}}{d\hat{t}_1 d\hat{u}_1} + \sum_{q=u,d,s} F_q^\gamma(x, Q^2) \left\{ F_q^A(x_2, Q^2, \vec{b}, z) + F_{\overline{q}}^A(x_2, Q^2, \vec{b}, z) \right\} \hat{s}^2 \frac{d^2\sigma_{q\overline{q}}}{d\hat{t}_1 d\hat{u}_1} \right]$$

Parton Distribution Functions in the Photon

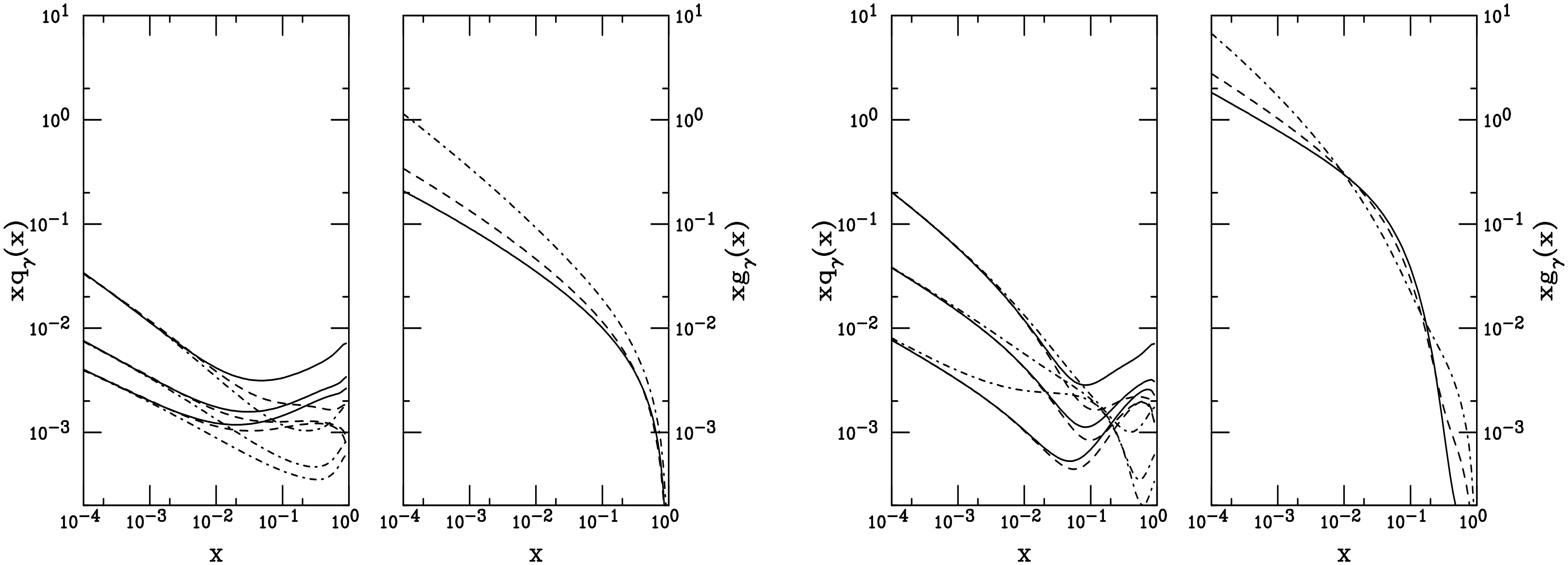

Figure 1: We show the GRV-G LO (left) and LAC1 (right) quark (a) and gluon (b) distributions of the photon. In (a) the up (solid), down (dashed) and strange (dot-dashed) distributions are evaluated at $2m_c$ (lower curves), m_b (middle curves) and m_t (upper curves). In (b) the gluon distributions are shown at $2m_c$ (solid), m_b (dashed) and m_t (dot-dashed).

Shadowing Parameterizations

Compare EKS98 and FGS

Recent parameterization by Frankfurt *et al* also shown, uses EKS98 for valence shadowing, stronger gluon shadowing at low x, cuts off modification above $x = 0.25$ for sea, 0.03 for gluon

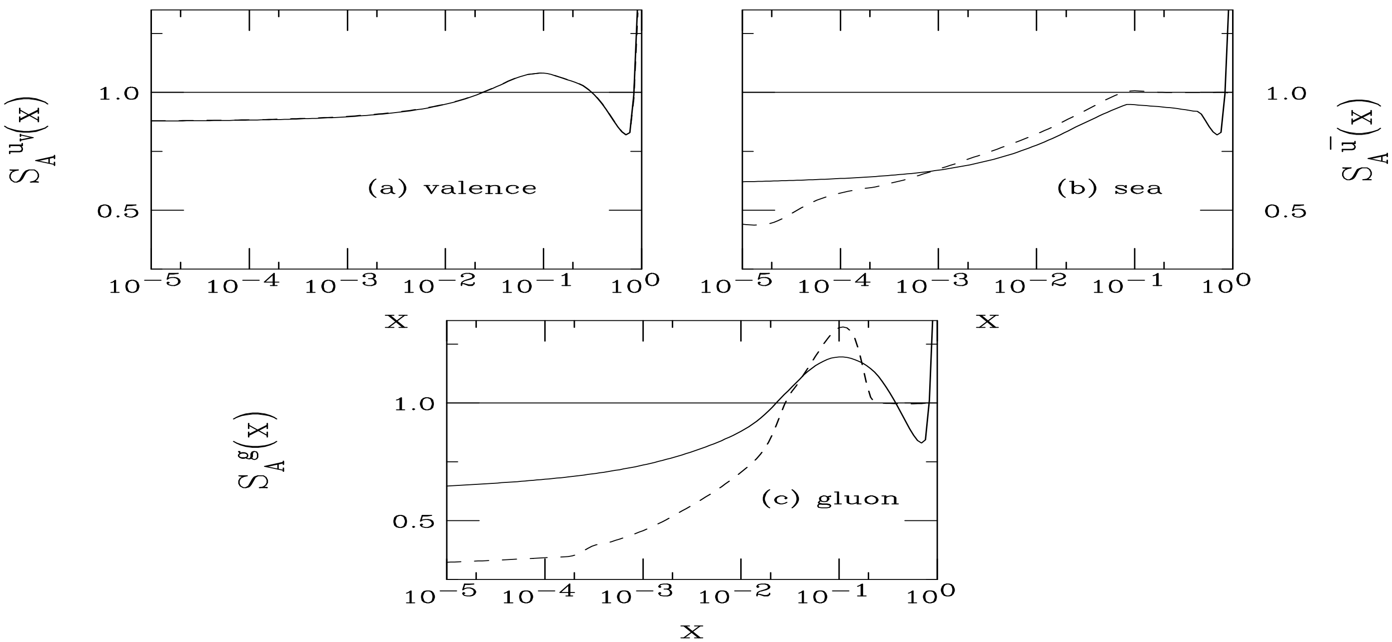

Figure 2: The EKS98 and FGS shadowing parameterizations are compared at the scale $\mu = 2m_c = 2.4$ GeV. The solid curves are the EKS98 parameterization, the dashed, FGS.

Heavy Quark Production Diagrams

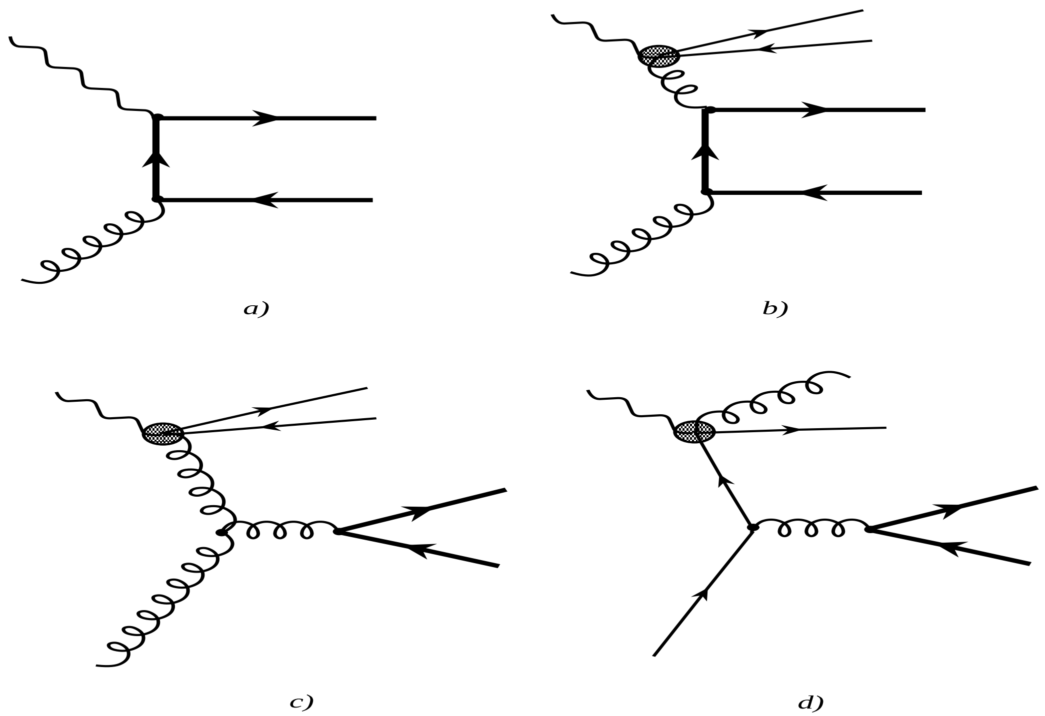

Figure 3: Feynman diagrams for heavy quark photoproduction for (a) direct and (b)-(e) resolved photons.

$Q\overline{Q}$ Photoproduction at RHIC

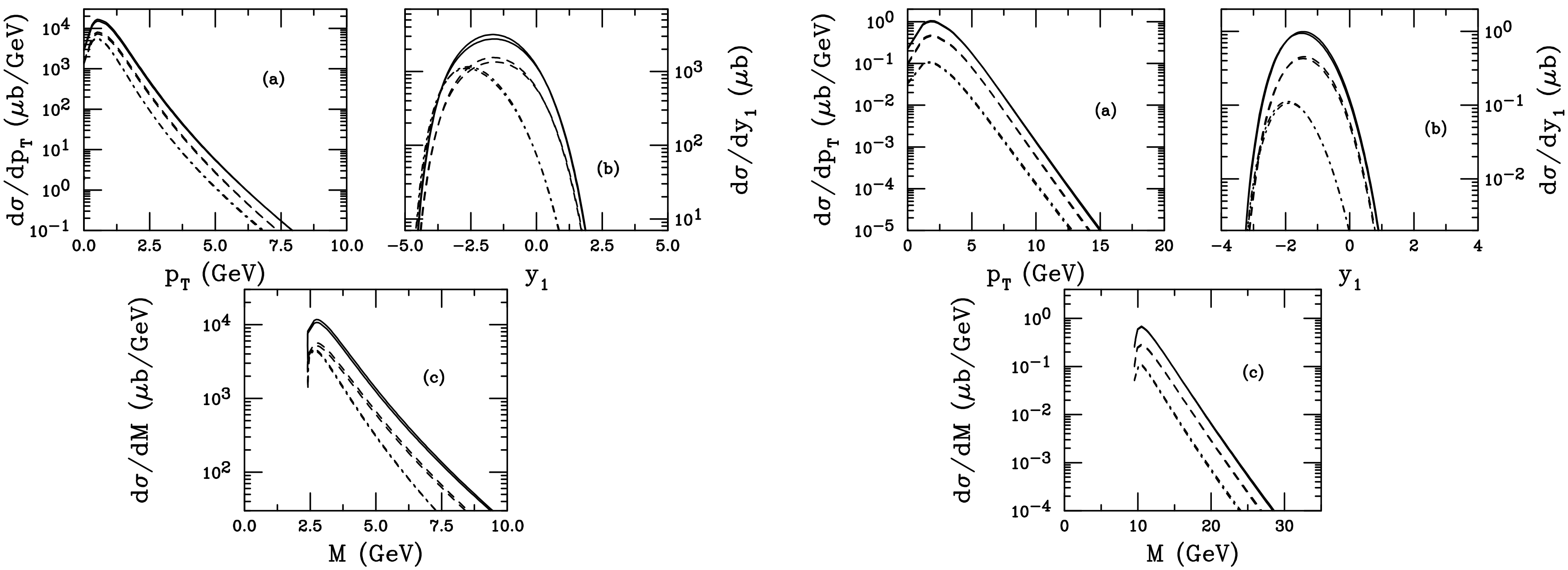

Figure 4: Charm (left) and bottom (right) photoproduction in peripheral Au+Au collisions at RHIC for $b > 2R_A$. The single quark p_T (a) and rapidity (b) distributions are shown along with the $c\overline{c}$ pair invariant mass (c). The direct (dashed), resolved (dot-dashed), and the sum of the two (solid) are shown. The direct contribution is divided by two to distinguish it from the total while the resolved charm contribution is multiplied by ten (the bottom resolved contribution is unchanged). There are two curves for each contribution: no shadowing and EKS98. At this energy, the curves are almost indistinguishable but the curves with shadowing are somewhat higher, especially at negative rapidities. In the rapidity distributions, the photon is coming from the left. With J. Nystrand and S. Klein.

Direct $Q\overline{Q}$ Photoproduction at the LHC

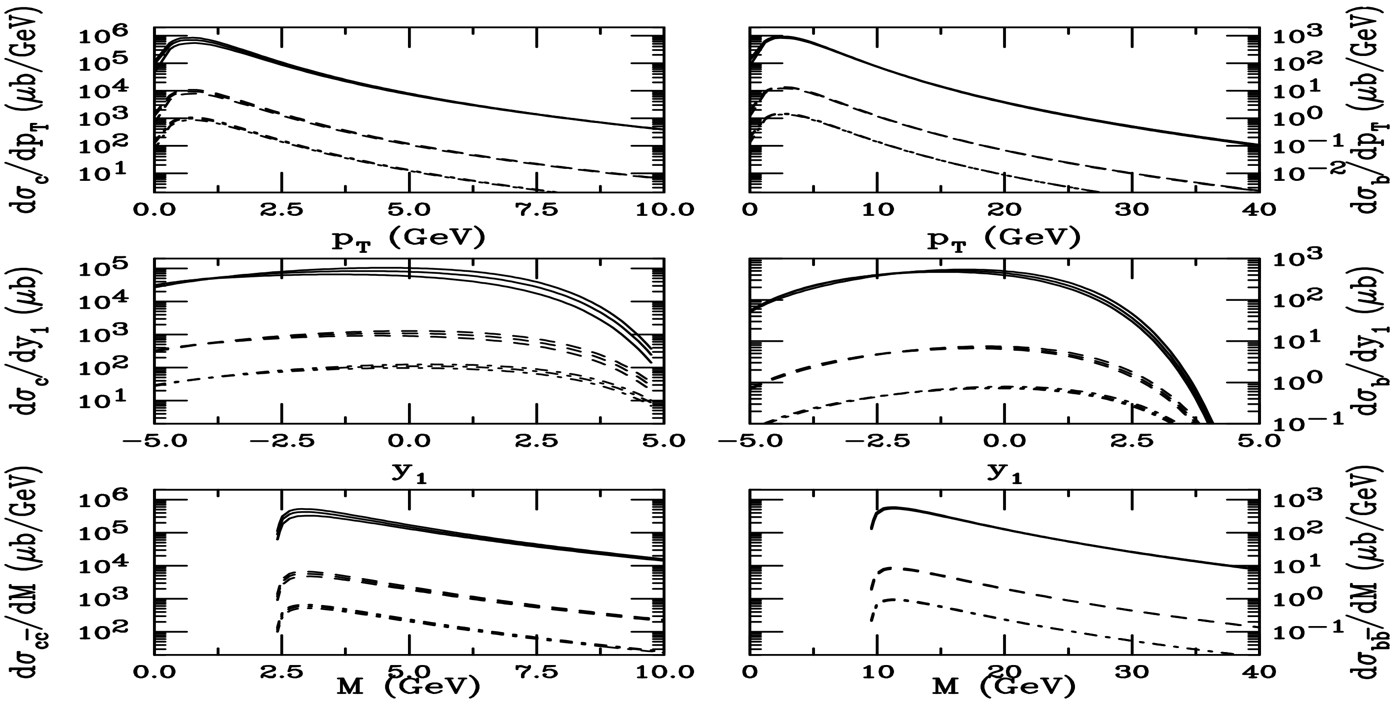

Figure 5: Direct $Q\overline{Q}$ photoproduction in peripheral AA collisions. The left-hand side is for charm while the right-hand side is for bottom. The single Q p_T (upper) and rapidity (middle) distributions are shown along with the $Q\overline{Q}$ pair invariant mass distributions (lower). The O+O (dot-dashed), Ar+Ar (dashed) and Pb+Pb (solid) results are given. There are three curves for each contribution: no shadowing, EKS98 and FGS. At $y_1 > 0$, the highest curve is without shadowing, the middle curve with EKS98 and the lower curve with FGS. The photon is coming from the left. With J. Nystrand and S. Klein.

Shadowing Effects on $Q\overline{Q}$ Photoproduction

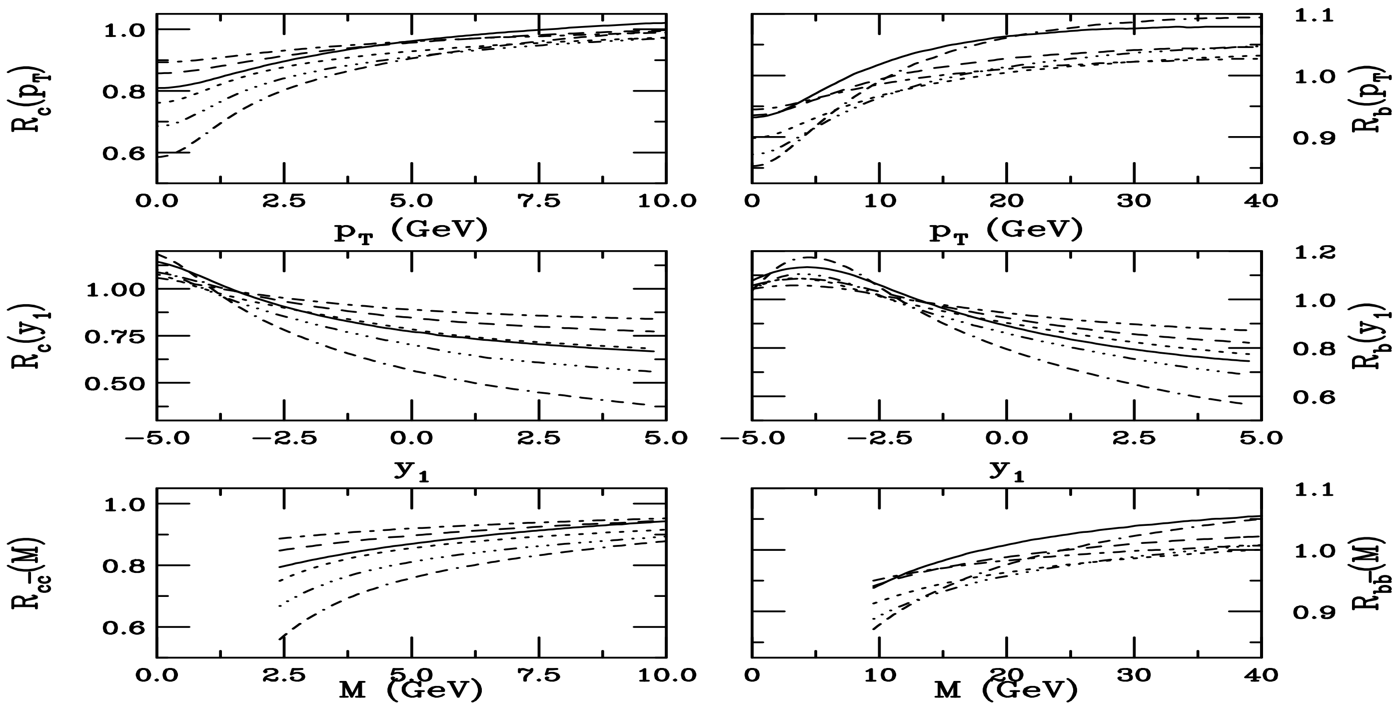

Figure 6: Shadowing in direct $Q\overline{Q}$ photoproduction in peripheral AA collisions. The left-hand side shows the results for charm while the right-hand side gives the results for bottom. The single Q p_T (upper) and rapidity (middle) ratios are shown along with the $Q\overline{Q}$ pair invariant mass ratios (lower). The results for the EKS98 (O+O (dot-dashed), Ar+Ar (dashed) and Pb+Pb (solid)) and FGS (O+O (dotted), Ar+Ar (dot-dot-dot-dashed) and Pb+Pb (dash-dash-dash-dotted)) shadowing parameterizations are given. The photon is coming from the left.

Average x Values for $Q\overline{Q}$ Photoproduction

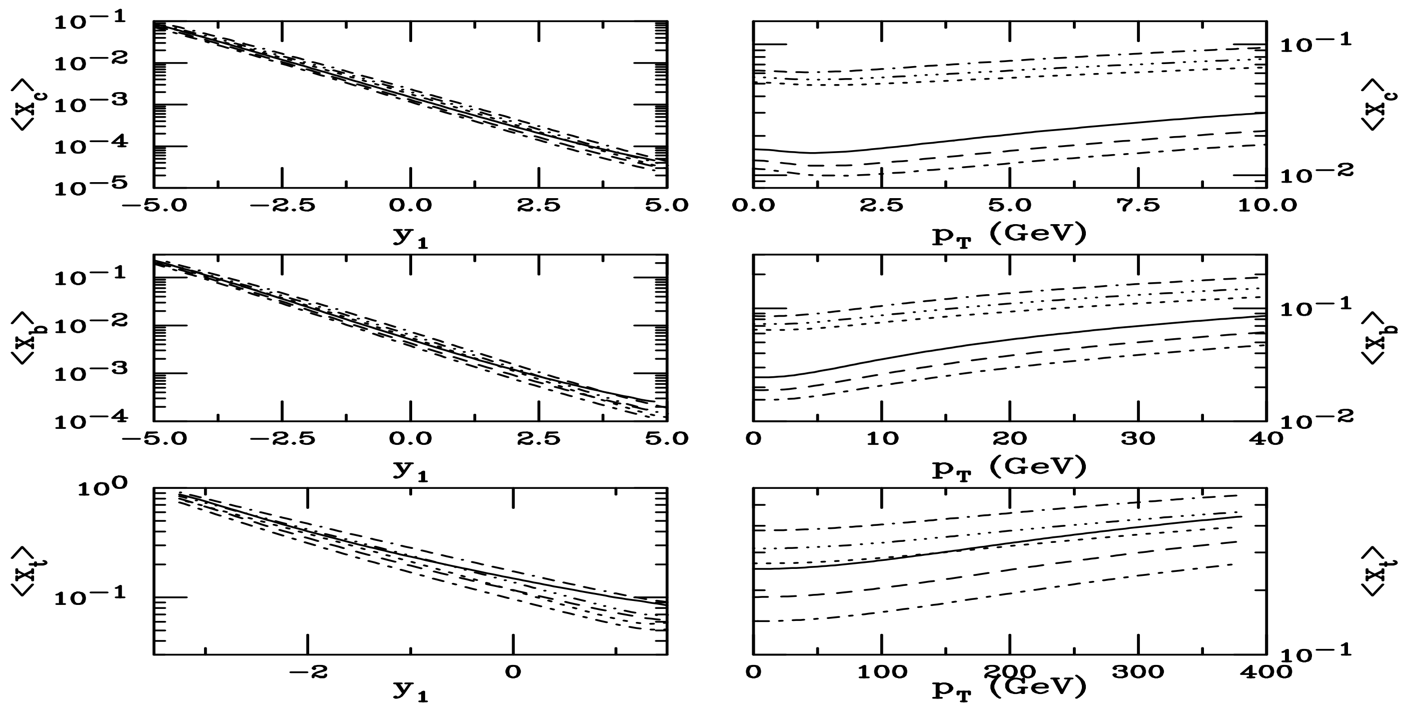

Figure 7: The average value of the nucleon parton momentum fraction x as a function of quark rapidity (left-hand side) and transverse momentum (right-hand side). The results are given for charm (upper), bottom (middle) and top (lower). The direct values are given for O+O (dot-dashed), Ar+Ar (dashed) and Pb+Pb (solid) while the resolved values are given for O+O (dotted), Ar+Ar (dot-dot-dot-dashed) and Pb+Pb (dash-dash-dash-dotted). (Resolved production is calculated with the GRV-G photon parton distributions.) The photon is coming from the left.

Direct $Q\overline{Q}$ Photoproduction Cross Sections

	$\sigma^{\rm dir}$ (mb)		
AA	no shad	EKS98	FGS
	$c\overline{c}$		
O+O	1.66	1.50	1.35
Ar+Ar	16.3	14.3	12.3
Pb+Pb	1246	1051	850
	$b\overline{b}$		
O+O	0.0081	0.0078	0.0075
Ar+Ar	0.073	0.070	0.066
Pb+Pb	4.89	4.71	4.42
	$t\overline{t}$		
O+O	9.13×10^{-9}	9.27×10^{-9}	9.31×10^{-9}
Ar+Ar	2.86×10^{-8}	2.88×10^{-8}	2.87×10^{-8}
Pb+Pb	3.29×10^{-7}	3.21×10^{-7}	3.22×10^{-7}

Table 2: Direct $Q\overline{Q}$ photoproduction cross sections integrated over $b > 2R_A$ in peripheral AA collisions. With J. Nystrand and S. Klein.

Resolved $Q\overline{Q}$ Photoproduction

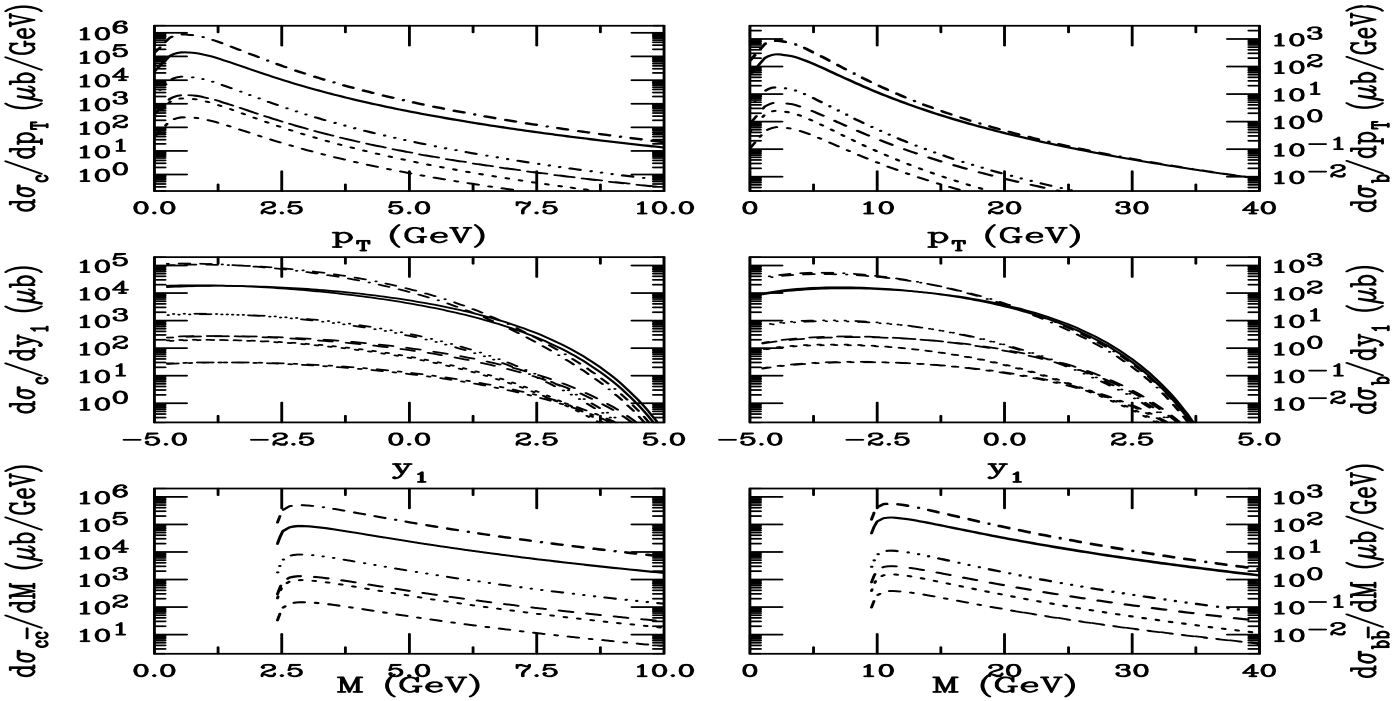

Figure 8: Resolved $Q\overline{Q}$ photoproduction in peripheral AA collisions. The left-hand side shows the results for charm while the right-hand side gives the results for bottom. The single Q p_T (upper) and rapidity (middle) distributions are shown along with the $Q\overline{Q}$ pair invariant mass distributions (lower). The results for the GRV-G (O+O (dot-dashed), Ar+Ar (dashed) and Pb+Pb (solid)) and LAC1 (O+O (dotted), Ar+Ar (dot-dot-dot-dashed) and Pb+Pb (dash-dash-dash-dotted)) photon parton densities are given. There are two curves for each contribution: no shadowing and EKS98. At $y_1 > 0$, the highest curve is without shadowing. The photon is coming from the left. With J. Nystrand and S. Klein.

Shadowing in Resolved $Q\overline{Q}$ Photoproduction

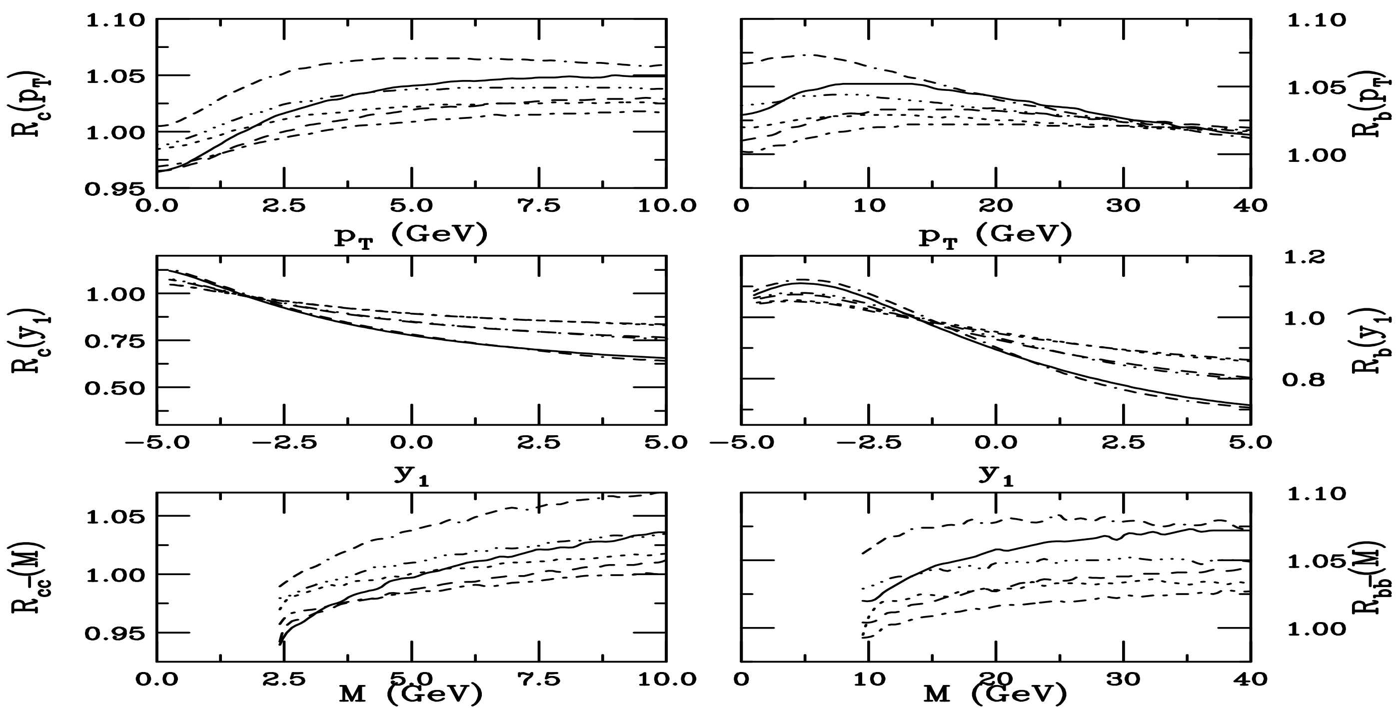

Figure 9: Shadowing in resolved $Q\overline{Q}$ photoproduction in peripheral AA collisions. The left-hand side shows the results for charm while the right-hand side gives the results for bottom. The EKS98 shadowing parameterization is used in both cases. The single Q p_T (upper) and rapidity (middle) ratios are shown along with the $Q\overline{Q}$ pair invariant mass ratios (lower). The results for the GRV-G (O+O (dot-dashed), Ar+Ar (dashed) and Pb+Pb (solid)) and LAC1 (O+O (dotted), Ar+Ar (dot-dot-dot-dashed) and Pb+Pb (dash-dash-dash-dotted)) photon parton distributions are given. The photon is coming from the left.

Relative Direct to Resolved $Q\overline{Q}$ Photoproduction

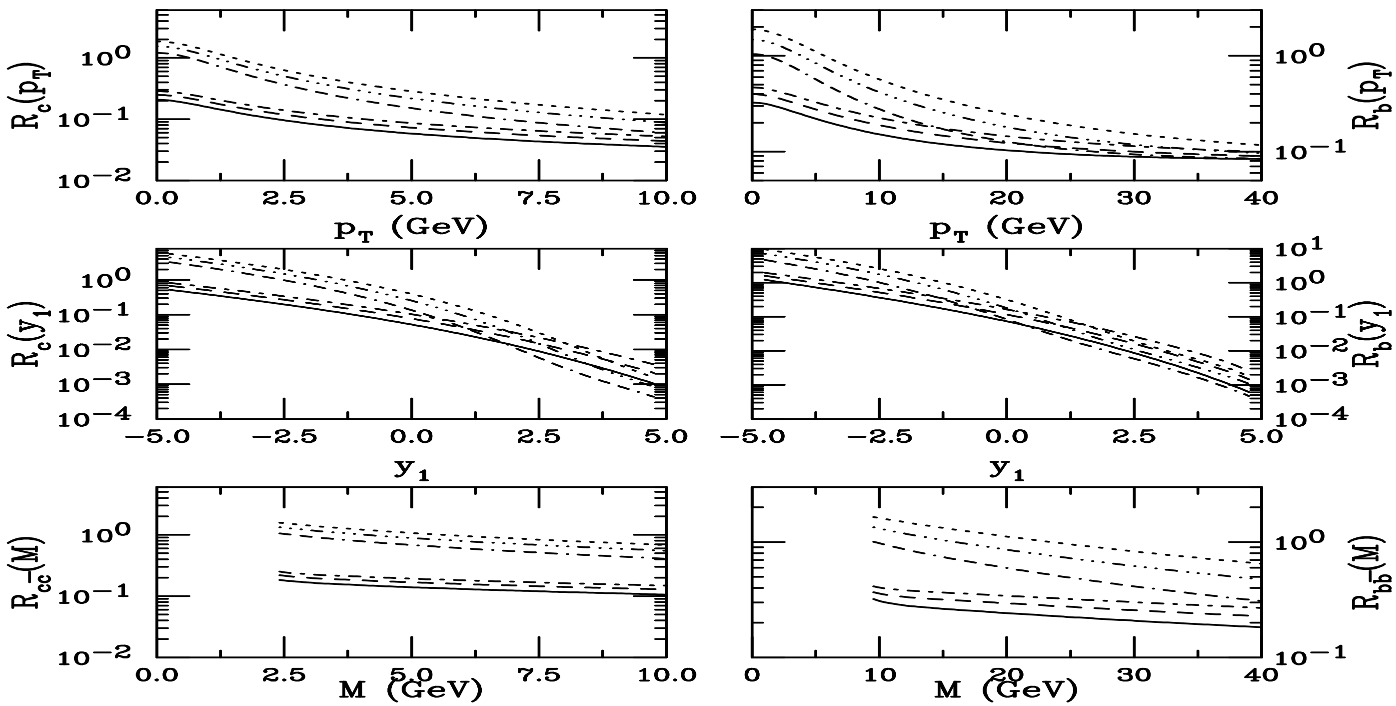

Figure 10: Resolved to direct $Q\overline{Q}$ photoproduction ratio in peripheral AA collisions. The left-hand side shows the results for charm while the right-hand side gives the results for bottom. The EKS98 shadowing parameterization is used in both cases. The single Q p_T (upper) and rapidity (middle) ratios are shown along with the $Q\overline{Q}$ pair invariant mass ratios (lower). The results for the GRV-G (O+O (dot-dashed), Ar+Ar (dashed) and Pb+Pb (solid)) and LAC1 (O+O (dotted), Ar+Ar (dot-dot-dot-dashed) and Pb+Pb (dash-dash-dash-dotted)) photon parton distributions are given. The photon is coming from the left.

Resolved $Q\overline{Q}$ Photoproduction Cross Sections

	GRV			LAC1	
AA	no shad	EKS98	FGS	no shad	EKS98
			$c\overline{c}$		
O+O	0.351	0.346	0.331	2.04	2.02
Ar+Ar	3.00	2.93	2.77	16.6	16.6
Pb+Pb	190.0	186.7	174.3	987	1007
			$b\overline{b}$		
O+O	0.0029	0.0029	0.0029	0.0105	0.0106
Ar+Ar	0.0222	0.0226	0.0024	0.073	0.075
Pb+Pb	1.21	1.26	1.25	3.41	3.66
			$t\overline{t}$		
O+O	2.81×10^{-10}	2.76×10^{-10}	–	2.92×10^{-10}	2.88×10^{-10}
Ar+Ar	1.08×10^{-9}	1.04×10^{-9}	–	1.09×10^{-9}	1.05×10^{-9}
Pb+Pb	1.60×10^{-8}	1.48×10^{-8}	–	1.62×10^{-8}	1.49×10^{-8}

Table 3: Resolved $Q\overline{Q}$ photoproduction cross sections integrated over $b > 2R_A$ in peripheral AA collisions. With J. Nystrand and S. Klein.

Composition of Resolved Contribution

Resolved contribution can be significant, depending on parameterization of photon PDFs

Large q and $\overline{q}$ densities in the photon at large x means that $q\overline{q}$ annihilation is an important component of resolved production, bigger for GRV than LAC1

GRV: $c\overline{c}$ is 4% $q\overline{q}$, $b\overline{b}$ is 10%

LAC1: $c\overline{c}$ is $1-2\%$ $q\overline{q}$, $b\overline{b}$ is $4-7\%$

x_2 and p_T Reach of Direct Pb+Pb $b\bar{b}$ Photoproduction

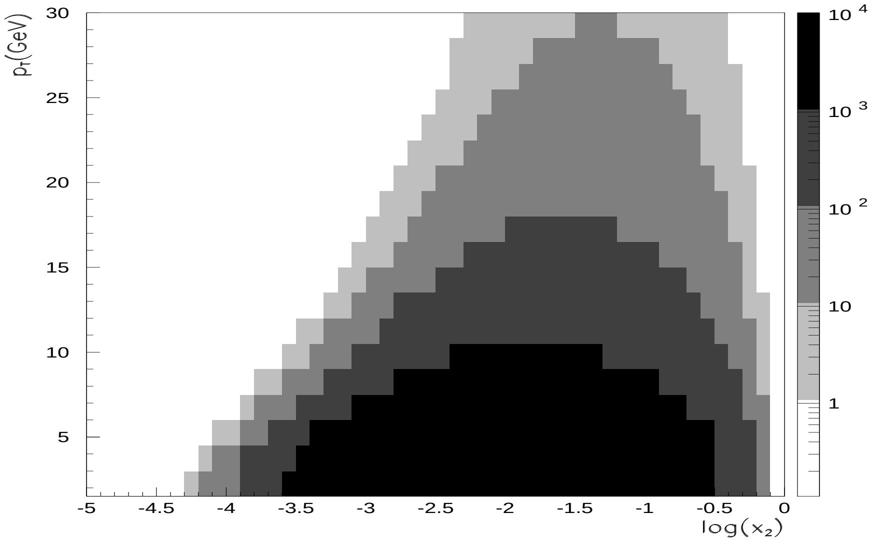

Figure 11: The rate for direct inclusive $b\bar{b}$ photoproduction for a one month LHC Pb+Pb run at $0.42 \times 10^{27}\text{cm}^{-2}\text{s}^{-1}$. Rates are in counts per bin of $\pm 0.25 x_2$ and ± 0.75 GeV in p_T. With M. Strikman and S. White.

Heavy Quark Photoproduction in pA

Calculations done in the equal speed frame

This doesn't make any difference at RHIC because the proton energy is tunable, $\sqrt{S}$ is the same in pA and AA

At LHC we assume that the proton beam is used at its maximum energy, 7 TeV so pA energy is higher

Using pA photoproduction to measure the nuclear gluon distribution tricky because differences in flux between pA and AA must be taken into account

In photon flux, $w_R^{AA} > w_R^{pA}$, so that $c\overline{c}$ in AA is 22-37% smaller at the same energy, $b\overline{b}$ is 37-65% smaller (both calculated using analytical formula for the flux)

Difference between pA and AA least for small A where $R_A - r_p$ is small

Difference largest for $b\overline{b}$ because close to threshold

Direct and Resolved $Q\overline{Q}$ pA Photoproduction Cross Sections

pA	$\sigma^{\rm dir}$ (μb)	$\sigma^{\rm res}$(GRV) (μb)	$\sigma^{\rm res}$(LAC1) (μb)
		$c\overline{c}$	
pO	75.5	19.7	120.6
pAr	335	81.1	486.3
pPb	5492	1160	6371
		$b\overline{b}$	
pO	0.419	0.190	0.773
pAr	1.775	0.739	2.886
pPb	26.83	9602	34.68
		$t\overline{t}$	
pO	1.54×10^{-6}	4.00×10^{-8}	4.00×10^{-8}
pAr	4.40×10^{-6}	1.23×10^{-7}	1.24×10^{-7}
pPb	3.00×10^{-5}	9.74×10^{-7}	9.86×10^{-7}

Table 4: Direct and resolved $c\overline{c}$ and $b\overline{b}$ photoproduction cross sections integrated over $b > r_p + R_A$ in pA collisions at the LHC.

x_2 and p_T Reach of Direct pPb $b\bar{b}$ Photoproduction

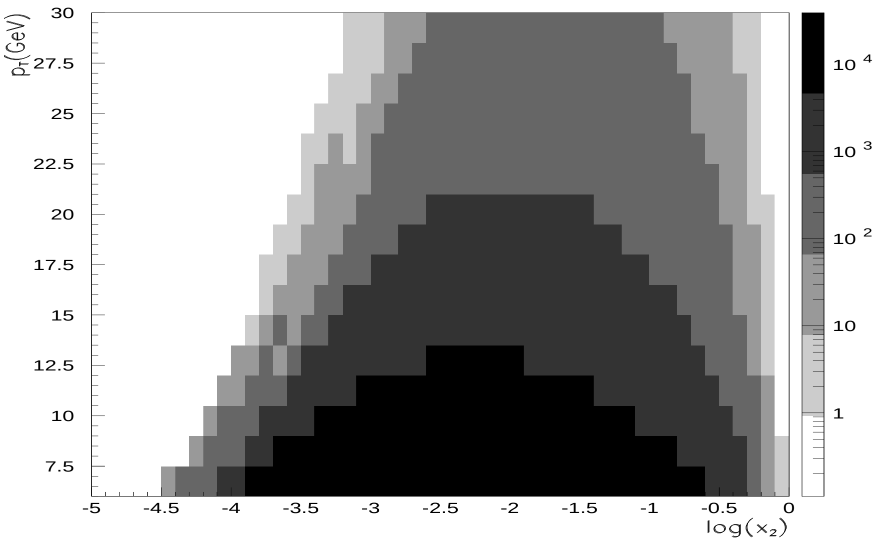

Figure 12: The expected inclusive $b\bar{b}$ photoproduction rate in a one month LHC pPb run at $7.4 \times 10^{29}\mathrm{cm}^{-2}\mathrm{s}^{-1}$. Rates are in counts per bin of $\pm 0.25 x_2$ and ± 0.75 GeV in p_T. With M. Strikman and S. White.

Dijet Production Diagrams

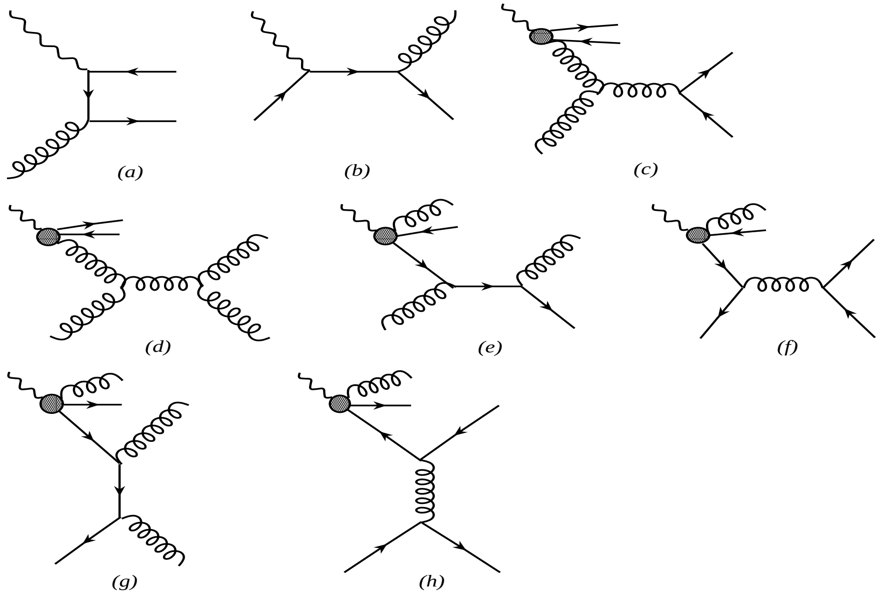

Figure 13: Feynman diagrams for dijet photoproduction from direct, (a) and (b), and resolved photons, (c)-(h). Only a sample of the resolved diagrams are shown. Crossed diagrams are not shown.

Photon + Jet Production Diagrams

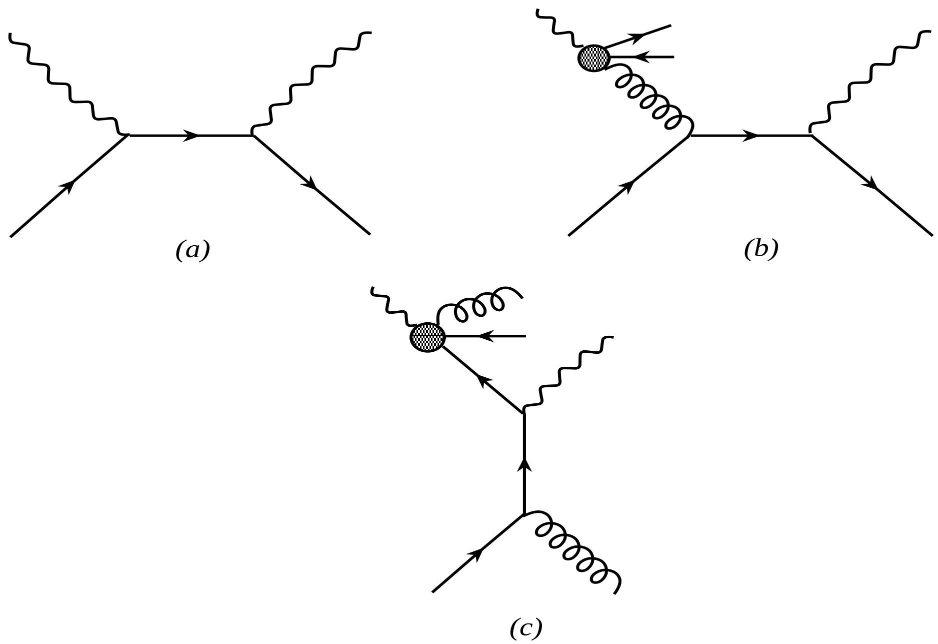

Figure 14: Feynman diagrams for γ+jet photoproduction from direct, (a), and resolved photons, (b) and (c). Crossed diagrams are not shown.

Jet Photoproduction at LHC

Direct jet photoproduction an easy extension of this calculation, same photon-gluon fusion diagrams, $m_Q \to 0$ plus also QCD Compton diagram

Include fragmentation through KKP determination from e^+e^- data at LEP

Fragmentation functions assume factorization and universality, same as initial state parton distribution

Resolved jet photoproduction includes all $2 \to 2$ processes, gives larger contribution than direct photoproduction at low p_T

Direct Dijet Photoproduction

Hadronic reaction: $\gamma(k)+N(P_2) \rightarrow \mathrm{jet}(p_1) + \mathrm{jet}(p_2) + X$

LO partonic reactions: $\gamma(k) + g(x_2P_2) \rightarrow q(p_1) + \overline{q}(p_2)$

$\gamma(k) + q(x_2P_2) \rightarrow g(p_1) + q(p_2)$

Partonic cross section

$$s^2\frac{d^2\sigma_{\gamma g\rightarrow q\overline{q}}}{dtdu} = \pi\alpha_s(\mu^2)\alpha e_Q^2[\frac{t^2+u^2}{tu}]\delta(s+t+u) \ ,$$

$$s^2\frac{d^2\sigma_{\gamma q\rightarrow gq}}{dtdu} = -\frac{8}{3}\pi\alpha_s(\mu^2)\alpha e_Q^2[\frac{s^2+t^2}{st}]\delta(s+t+u)$$

Partonic invariants: $s = (k+x_2P_2)^2 = 4kx_2m_p\gamma_L$, $t = (x_2P_2-p_1)^2$, $u = (k-p_1)^2$

Hadronic cross section, convolution over parton density, photon flux

$$S_{NN}^2\frac{d^2\sigma^{\rm dir}_{\gamma A\rightarrow {\rm jet+jet}+X}}{dTdUd^2b} = 2\int dz \int_{k_{\rm min}}^{\infty} dk\frac{d^3N_\gamma}{dkd^2b}\int_{x_{2_{\rm min}}}^1\frac{dx_2}{x_2}[\sum_{i,j,l=q,\overline{q},g}F_i^A(x_2,\mu^2,\vec{b},z)s^2\frac{d^2\sigma_{\gamma i\rightarrow jl}}{dtdu}] \quad (1)$$

Hadronic invariants: $S = (k+P_2)^2$, $T = (P_2-p_1)^2$, $U = (k-p_1)^2$, **Now** $T = -\sqrt{S_{NN}}p_Te^{-y_1}$ **and** $x_1 = (p_T/\sqrt{S_{NN}})(e^{y_1}+e^{y_2})$ **and** $x_2 = (p_T/\sqrt{S_{NN}})(e^{-y_1}+e^{-y_2})$ **since no mass scale**

Direct Dijet Photoproduction

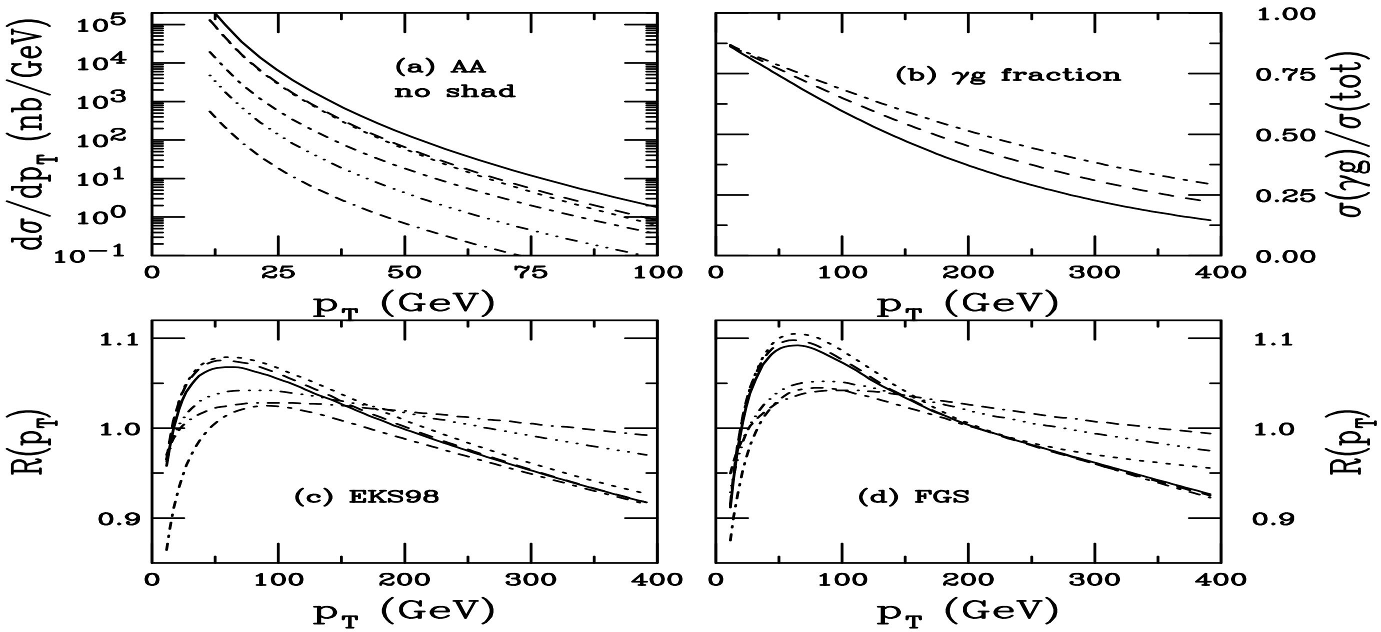

Figure 15: Direct jet photoproduction in peripheral collisions. (a) The p_T distributions for $|y_1| \leq 1$ are shown for AA collisions. The solid curves is the total for Pb ions while the produced quarks (dashed), antiquarks (dotted) and gluons (dot-dashed) are shown separately. The total production for Ar (dot-dot-dot-dashed) and O (dot-dash-dash-dashed) ions are also shown. (b) The fraction of gluon-initiated jets as a function of p_T for Pb+Pb (solid), Ar+Ar (dashed) and O+O (dot-dashed) interactions. (c) The EKS98 shadowing ratios for produced partons. The solid curve is the total for Pb ions while the ratios for produced quarks (dashed), antiquarks (dotted) and gluons (dot-dashed) are shown separately. The total ratios for Ar (dot-dot-dot-dashed) and O (dot-dash-dash-dashed) ions are also shown. (d) The same as (c) for FGS.

Final-state Hadrons From Dijet Photoproduction

Same reactions as before, now jets hadronized

$$\frac{d\sigma^{\rm dir}_{\gamma A\to hX}}{dp_T d^2b} = 4p_T \int dz \int_{\theta_{\rm min}}^{\theta_{\rm max}} \frac{d\theta_{\rm cm}}{\sin\theta_{\rm cm}} \int dk \frac{d^3N_\gamma}{dk d^2b} \int \frac{dx_2}{x_2}$$
$$\times \Big[\sum_{i,l=q,\overline{q},g} F_i^A(x_2,\mu^2,\vec{b},z) \frac{d\sigma_{\gamma i\to lX'}}{dt} \frac{D_{h/l}(z_c,\mu^2)}{z_c} \Big]$$

X on left-hand side includes all final-state hadrons in addition to h, X' on right-hand side is unobserved final-state parton

The subprocess cross sections, $d\sigma/dt$, are related to $s^2 d\sigma/dtdu$ through $\delta(s+t+u)$ and division by s^2

Integral over rapidity replaced by an integral over center-of-mass scattering angle, $\theta_{\rm min} \leq \theta_{\rm cm} \leq \theta_{\rm max}$, corresponding to a given rapidity cut: $\theta_{\rm min} = 0$ and $\theta_{\rm max} = \pi$ covers all rapidity; $\theta_{\rm min} = \pi/4$ and $\theta_{\rm max} = 3\pi/4$ is about $|y_1| \leq 1$

KKP fragmentation functions with $\mu^2 = p_T^2$

Resolved rates not shown, higher at low p_T but become comparable and then lower than direct as p_T increases

Final-State Hadron Production

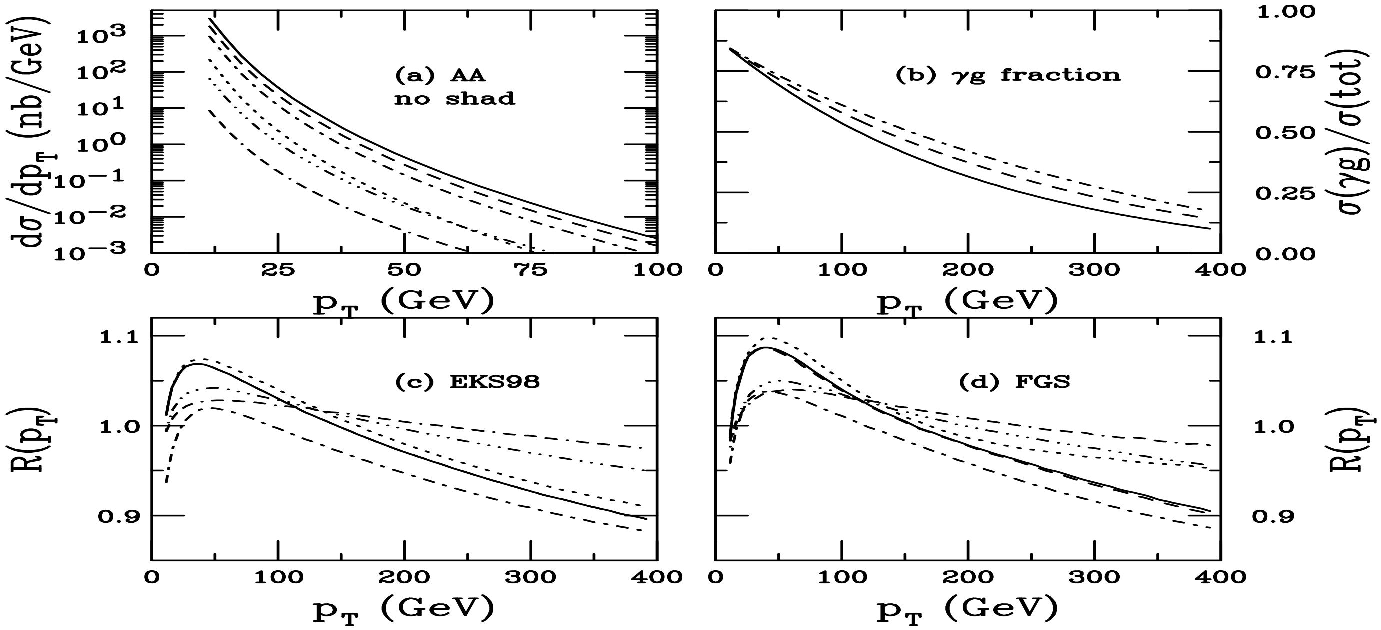

Figure 16: Direct photoproduction of leading hadrons in peripheral collisions. (a) The p_T distributions for $|y_1| \leq 1$ are shown for AA collisions. The solid curve is the total for Pb+Pb while the produced pions (dashed), kaons (dot-dashed) and protons (dotted) are shown separately. The total production for Ar+Ar (dot-dot-dot-dashed) and O+O (dot-dash-dash-dashed) are also shown. (b) The fraction of gluon-initiated hadrons as a function of p_T. The curves are the same as in (a). (c) The EKS98 shadowing ratios for produced pions. The solid curve is the total for Pb+Pb while the ratios for pions produced by quarks (dashed), antiquarks (dotted) and gluons (dot-dashed) are shown separately. The total ratios for Ar+Ar (dot-dot-dot-dashed) and O+O (dot-dash-dash-dashed) are also shown. (d) The same as (c) for FGS.

Average x Values for Dijet Photoproduction

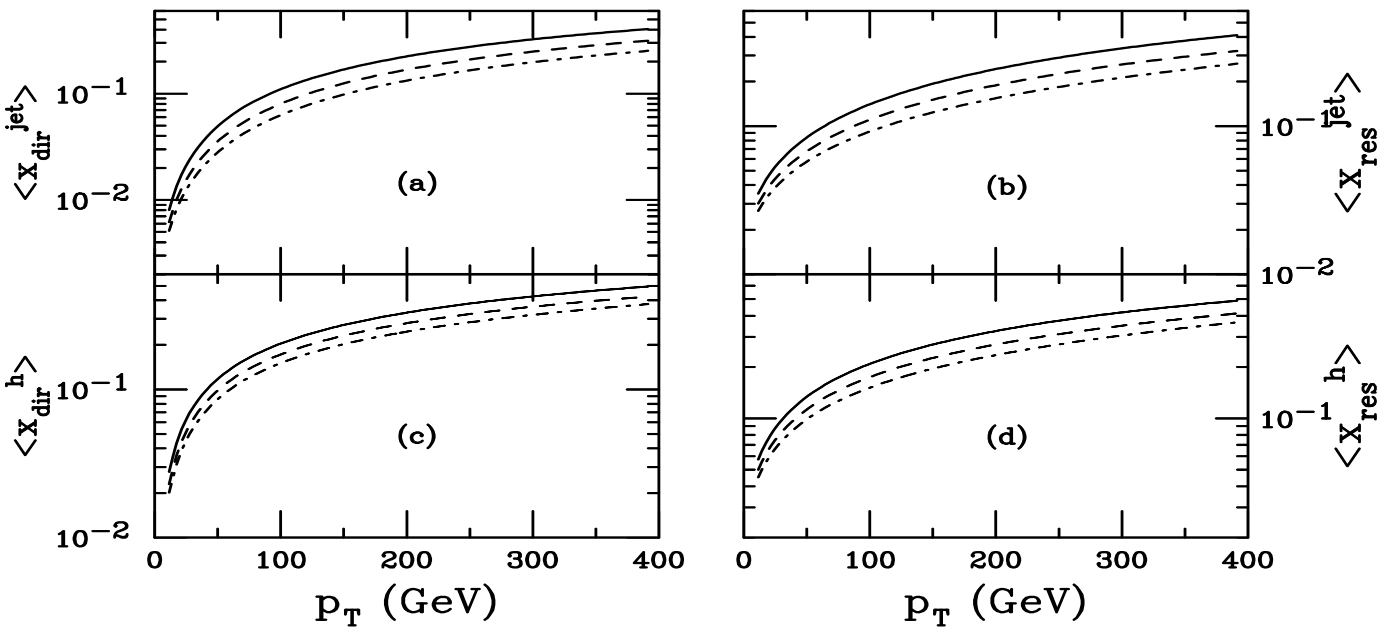

Figure 17: The average value of the nucleon parton momentum fraction x as a function of transverse momentum. Results are given for (a) direct and (b) resolved gluon jet production and for (c) direct and (d) resolved pion production by gluons. The results are given for O+O (dot-dashed), Ar+Ar (dashed) and Pb+Pb (solid) interactions.

Dijet Rates in x and p_T

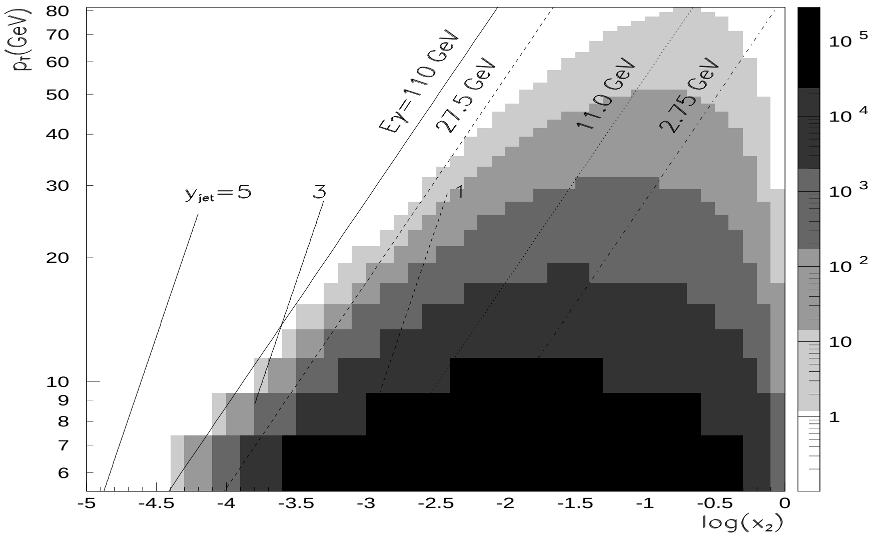

Figure 18: The expected inclusive dijet photoproduction rate for a one month LHC Pb+Pb run at $0.42 \times 10^{27}\text{cm}^{-2}\text{s}^{-1}$. Rates are in counts per bin of $\pm 0.25 x_2$ and ± 1 GeV in p_T.

Summary

- **We have calculated charm, bottom and top photoproduction in heavy ion collisions**
- **Resolved contribution is very sensitive to the photon parton density**
- **Rates are high with good reach in x for $b\bar{b}$ production**
- **We have also considered photoproduction of jets**
- **Dijet rates also high but best range of x achieved with not too high p_T jets**
- **Both processes can probe nuclear qluon distributions at low x and perturbative scales in relatively clean environment**